Swelling of a cluster phase in Langmuir monolayers containing semi-fluorinated phosphonic acids

Siwar Trabelsi,[a] Shishan Zhang,[b] T. Randall Lee[b] and Daniel K. Schwartz*[a]

Received 24th July 2007, Accepted 27th September 2007
First published as an Advance Article on the web 15th October 2007
DOI: 10.1039/b711286f

Langmuir monolayers of semi-fluorinated nonadecylphosphonic acid ($F8H11PO_3$), hexadecylphosphonic acid ($H16PO_3$), and their mixtures were investigated by Brewster angle microscopy (BAM), atomic force microscopy (AFM) and surface-pressure measurements. Nanometre-scale two-dimensional clusters were observed by AFM in a spread monolayer of pure $F8H11PO_3$ transferred to mica. Two different organized arrangements of clusters were observed. AFM and BAM observations showed that the mixture exhibits a solid phase over a large range of mole fraction and surface pressure, sometimes in coexistence with clusters. With increasing mole fraction of $H16PO_3$, the lateral shape of these clusters remains the same while their organization and their height change.

Introduction

Perfluorinated alkanes are both hydrophobic and lipophobic. At the most fundamental level, this bifunctional behavior arises from molecular interactions, both long- and short-ranged, that stem from the high electronegativity, low polarizability, and large atomic radius of fluorine relative to hydrogen. Semi-fluorinated alkanes, or amphiphilic derivatives, are comprised of two chemically and structurally distinct blocks covalently bound to form a single molecule. This arrangement leads to unique self-assembly behavior that might be useful in cosmetics[1] and in pharmaceutical applications[2] such as pulmonary drug delivery.

Monolayer domains with finite lateral size generally originate from the competition between or incompatibility of molecular interactions. For example, the competition between line tension at domain boundaries and electrostatic dipole–dipole repulsion results in stable macroscopic domains in two-phase lipid monolayers. In practice, these domains have characteristic length scales $\geqslant 1$ μm; however, in principle they could be nanoscale for vanishingly small values of line tension.[3]

The formation of nanoscale molecular clusters in thin films often arises from frustrated molecular packing and/or chemical dissimilarity. The research groups of Manne[4,5] and Ducker[6,7] have published extensive studies of surface micelles formed by wedge-shaped (*i.e.*, micelle-forming) surfactants at the interface of aqueous solution and a solid surface. These clusters display a radius of curvature related to the molecular length, as observed with three-dimensional micelles. We have observed analogous behavior in reverse-micelle-forming surfactants at the interface between a solid and a solution with a non-polar solvent.[8,9] In these cases, the tendency of the surfactant molecules to form curved aggregates was frustrated by the presence of a planar substrate, leading to periodic arrays of clusters (spherical or cylindrical surface micelles).

The chemical dissimilarity between hydrocarbons and fluorocarbons is known to induce phase separation in many situations. For example, binary mixtures of hydrocarbon and perfluorinated surfactants[10] exhibit highly nonideal behavior (*e.g.*, phase separation) at the air–water interface[11] or in LB films.[8] Such mixtures have also been reported to form two types of micelles simultaneously in solution – one rich in fluorocarbon and the other rich in hydrocarbon.[12] The miscibility of fluorocarbon and hydrocarbon amphiphiles is highly sensitive to their chemical structure. The stronger the headgroup–headgroup interactions, the better mutual miscibility of the amphiphiles is observed.[13] Lehmler *et al.* have reported some miscibility for mixtures of partially fluorinated carboxylic acids with dipalmitoylphosphatidylcholine (DPPC) at the air–water interface. Similar behavior has been observed for a mixture of partially fluorinated carboxylic acids and their respective hydrocarbon analogues.[11]

When grafted together in the same molecule, the chemical dissimilarity between fluorocarbon and hydrocarbon can lead to unusual molecular and supermolecular structures. For monolayers of semi-fluorinated carboxylic acids in the temperature range of 4–30 °C, it has been shown that perfluorinated segments pack in a simple hexagonal array with their long axes nearly perpendicular to the surface, with a helical twist structure superimposed on the all-*trans* zigzag conformation of the hydrocarbon chain.[14] Krafft and co-workers have observed that semi-fluorinated alkanes transferred onto silicon wafers form monodisperse surface micelles.[15] They found that the hydrocarbon blocks were in contact with the silicon and the fluorinated blocks were pointing outward.[16] In contrast with the observations of detergent surface micelles, the clusters of semi-fluorinated compounds displayed no organization or periodic behavior.

We believe that mixtures[17] of semi-fluorinated amphiphiles with hydrocarbon (or perfluorinated) amphiphiles might be

[a]*Department of Chemical and Biological Engineering, University of Colorado, Boulder, CO 80309-0424, USA. E-mail: Daniel.Schwartz@colorado.edu; Fax: +1 303-492-4341; Tel: +1 303-735-0240*
[b]*Department of Chemistry, University of Houston, Houston, TX 77204-5003, USA*

interesting because the latter component has the potential to "swell" the clusters formed by the semi-fluorinated component. This hypothesis motivated us to investigate whether the addition of a hydrocarbon component would influence the size, shape, and organization of these two-dimensional clusters. In the work reported here, Langmuir films of $H16PO_3$ and $F8H11PO_3$ and their mixture on a water subphase were investigated by BAM, while LB films on mica substrates were studied with AFM. Highly-organized two-dimensional clusters were observed for pure $F8H11PO_3$ transferred to mica. We discuss the influence of the addition of a hydrocarbon component ($H16PO_3$) on the size, height, and organization of these clusters.

Experimental

Materials

The strategy used to prepare 12,12,13,13,14,14,15,15,16,16,17,17,18,18,19,19,19-heptadecafluorononadecyl phosphonic acid (denoted as $F8H11PO_3$) is outlined in Scheme 1. Detailed procedures for each step are provided in the following paragraphs.

12,12,13,13,14,14,15,15,16,16,17,17,18,18,19,19,19-Heptadecafluorononadecanol, ($CF_3(CF_2)_7(CH_2)_{11}OH$; F8H11OH). This intermediate was synthesized *via* the radical addition of 1-iodoperfluorooctane to 10-undecen-1-ol. A 100 mL Schlenk flask equipped with a magnetic stirrer bar was charged with 2.00 g (11.7 mmol) of the alcohol, 200 mg of AIBN, and 6.40 g (12.0 mmol) of iodoperfluorooctane. The flask was sealed and submerged in liquid nitrogen to freeze the contents for degassing. After 10 minutes of submergence in the liquid nitrogen, the flask was evacuated and purged with argon 3 times. The flask was evacuated again and heated at 100 °C for 12 hours with stirring. The flask was then cooled to room temperature and an additional 200 mg of AIBN was added to the flask, which was again sealed, evacuated, and purged with argon 3 times. The flask was then evacuated and heated at 100 °C for 3 more hours with stirring. The reaction was cooled to room temperature, and 75 mL of glacial acetic acid was added to the reaction mixture. The contents of the Schlenk flask were then poured into a 500 mL round-bottomed flask containing 20 molar equivalents of powdered zinc (15.0 g). This mixture was allowed to stir at room temperature for 12 hours. The solution was then vacuum-filtered through a Büchner funnel, and 1.0 M NaOH was added to the acidic solution until the mixture exhibited a neutral pH as indicated by pH paper. The mixture was extracted with diethyl ether (3 × 100 mL), and the combined organic layers were washed with water (2 × 50 mL), dried over magnesium sulfate, filtered, rotary evaporated, and recrystallized from hexane to give 2.07 g of F8H11OH (3.51 mmol, 30% yield). ^{1}H NMR (300 MHz, $CDCl_3$): δ = 3.64 (t, J = 6.6 Hz, 2H), 1.95–2.13 (m, 2H), 1.47–1.61 (m, 5H), 1.22–1.42 (m, 16H).

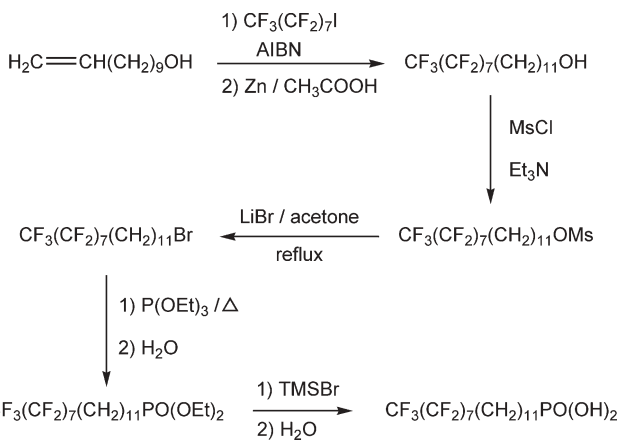

Scheme 1 Synthesis of terminally perfluorinated phosphonic acid, $F8H11PO_3$.

12,12,13,13,14,14,15,15,16,16,17,17,18,18,19,19,19-Heptadecafluorononadecyl-1-mesylate, ($CF_3(CF_2)_7(CH_2)_{11}OMs$; F8H11OMs). A 250 mL round-bottomed flask containing 100 mL of reagent grade hexane and a magnetic stirrer bar was charged with 2.07 g (3.51 mmol) of F8H11OH and 3 molar equivalents of triethylamine (1.50 mL). The flask was purged with argon for 5 minutes, and then methanesulfonyl chloride (0.54 mL; 7.0 mmol) was slowly added *via* syringe. The reaction mixture was allowed to stir at room temperature for 12 hours with the septum vented with a needle. Deionized water (100 mL) was added and allowed to hydrolyze the reaction for 30 minutes. The organic phase was then separated and washed with water (2 × 100 mL) and with brine (1 × 100 mL). The organic phase was dried over magnesium sulfate, filtered, rotary evaporated, and dried further on a Schlenk line to give 2.23 g of F8H11OMs (3.34 mmol, 95% yield). ^{1}H NMR (300 MHz, $CDCl_3$): δ = 4.22 (t, J = 6.6 Hz, 2H), 3.00 (s, 3H), 1.95–2.12 (m, 2H), 1.70–1.77 (m, 2H), 1.51–1.62 (m, 2H), 1.22–1.42 (m, 14H).

12,12,13,13,14,14,15,15,16,16,17,17,18,18,19,19,19-Heptadecafluorononadecyl bromide, ($CF_3(CF_2)_7(CH_2)_{11}Br$; F8H11Br). A 200 mL round-bottomed flask equipped with a magnetic stirrer bar was charged with 2.23 g (3.34 mmol) of F8H11OMs and 3 molar equivalents of lithium bromide (0.87 g). Reagent grade acetone (100 mL) was added, and the reaction mixture was refluxed for 12 hours. The reaction was cooled to rt, and the acetone removed by rotary evaporation. The crude product was washed with 50 mL of deionized water then extracted into reagent grade diethyl ether (3 × 20 mL). The organic phase was dried over magnesium sulfate, filtered, rotary evaporated, and further dried on a Schlenk line to give 2.12 g of F8H11Br (3.25 mmol, 97% yield). ^{1}H NMR (300 MHz, $CDCl_3$): δ = 3.41 (t, J = 7.1 Hz, 2H), 1.95–2.13 (m, 2H), 1.81–1.90 (quint, J = 7.2 Hz, 2H), 1.51–1.62 (m, 2H), 1.21–1.44 (m, 14H).

Diethyl 12,12,13,13,14,14,15,15,16,16,17,17,18,18,19,19,19-heptadecafluorononadecyl phosphonate, ($CF_3(CF_2)_7(CH_2)_{11}PO(OEt)_2$; $F8H11PO_3Et_2$). A 200 mL Schlenk flask equipped with a stirrer bar was charged with 2.12 g (3.25 mmol) of F8H11Br. The reaction flask was evacuated and purged several times with argon to remove moisture and air. Triethylphosphite (5.0 mL; 29 mmol) was then added *via*

syringe, and the reaction mixture was heated at 200 °C for 1 hour, cooled to room temperature, and stirred for an additional 12 hours. The reaction was quenched with the addition of 30 mL of deionized water, and then allowed to stir for another 24 hours. The resulting mixture was extracted with carbon tetrachloride (2 × 50 mL). The organic phase was washed with deionized water (2 × 50 mL) and brine (1 × 50 mL), dried over magnesium sulfate, filtered, rotary evaporated, and dried on a Schlenk line to give 1.39 g of $F8H11PO_3Et_2$ (1.96 mmol, 60% yield). ^{1}H NMR (300 MHz, $CDCl_3$): δ = 4.02–4.15 (m, 4H), 1.95–2.13 (m, 2H), 1.54–1.79 (m, 4H), 1.34 (t, J = 6.9 Hz, 6H), 1.22–1.43 (m, 16H).

12,12,13,13,14,14,15,15,16,16,17,17,18,18,19,19,19-Heptadecafluorononadecyl phosphonic acid, $(CF_3(CF_2)_7(CH_2)_{11}PO(OH)_2$; F8H11PO$_3$). A 200 mL Schlenk flask containing 1.39 g (1.96 mmol) of $F8H11PO_3Et_2$ was purged with argon for 10 minutes. Dry dichloromethane (50 mL) was then added *via* cannula, and trimethylsilyl bromide (TMSBr, 1.50 mL, 11.8 mmol) was added *via* syringe. The reaction mixture was stirred at room temperature for 12 hours. The solvent was then removed under vacuum on a Schlenk line, and 50 mL of deionized water was added. The mixture was allowed to stir at room temperature for another 12 hours. A large volume of ethyl acetate was required to extract the acid (3 × 500 mL). The organic phases were collected and dried over magnesium sulfate, filtered, rotary evaporated, and dried on a Schlenk line. The crude product was dissolved in a minimum amount of hot ethyl acetate, filtered hot, and then allowed to cool, giving 0.64 g (0.98 mmol, 50% yield) of recrystallized $F8H11PO_3$. ^{1}H NMR (300 MHz, TDF): δ = 2.10–2.23 (m, 2H), 1.51–1.61 (m, 6H), 1.30–1.50 (m, 14H). The poor solubility of the product precluded the collection of ^{13}C NMR data. HRMS Calcd for $C_{19}H_{24}F_{17}O_3P$: 654.1270. Found: 654.1285.

n-Hexadecyl phosphonic acid $C_{16}H_{33}PO(OH)_2$ (denoted as $H16PO_3$) was purchased from PolyCarbon Industries Inc. and used as received. Ultrapure water from a Millipore Milli-QUV system (resistivity 18.2 MΩ cm^{-1}) was used for the subphase of Langmuir monolayer. The pH of the subphase was adjusted to 3 by adding an aqueous solution of hydrochloric acid (Mallinckrodt). The spreading solutions for monolayer experiments were prepared by dissolving each component in tetrahydrofuran (Fisher Scientific) with a concentration of 1 mg mL^{-1} for $H16PO_3$ and 0.5 mg mL^{-1} for $F8H11PO_3$.

Brewster angle microscopy

A custom-built Brewster angle microscope (BAM) was used to visualize the monolayer structures at the air–water interface.[18,19] Light from a 30 mW, 670 nm diode laser was p-polarized by a Glan–Thomson prism before being directed to the air–water interface at an incident angle equal to the Brewster angle of water ($\theta_B \sim 53°$). The light reflected from the monolayer was focused onto a CCD camera by a 4× microscope objective after passing through an analyzer (a second Glan–Thomson prism). The images were recorded using a Hitachi CCD video camera.

Langmuir–Blodgett films

Langmuir monolayers were spread dropwise using a microlitre syringe at the air–water interface of a commercial Nima Langmuir–Blodgett trough. After spreading, the monolayers were left for 10 minutes to ensure solvent evaporation. The monolayers were compressed by a motorized barrier at a constant rate of 20 mm min^{-1}. The surface pressure was measured by the Wilhelmy plate method, using filter paper plates. LB films were transferred onto freshly-cleaved mica substrates by the upstroke mode of the vertical dipping method at a surface pressure of 4 or 20 mN m^{-1}. After deposition, LB films were stored in a small container for no more than 2 days.

Atomic force microscopy

The samples were imaged with a Nanoscope MMAFM (Digital Instruments – now Veeco). Images were obtained in contact mode using silicon nitride tips (196 μm long × 23 μm wide). All measurements were made at room temperature (23 ± 1 °C).

Results

Phases and phase diagrams

Two distinct arrangements of clusters, denoted C1 and C2, were observed, as was a laterally-homogeneous phase that we denote the S1 phase. The structural details of these phases will be presented below. BAM and AFM images were used to determine the conditions under which the phases exist and coexist. Fig. 1 summarizes this information in the form of a monolayer phase diagram of $H16PO_3$ and $F8H11PO_3$. The collapse pressures (represented by squares in the phase diagram) were deduced from the surface-pressure measurements. For $X_{F8H11PO_3} \geqslant 0.8$, two-dimensional clusters (C1 + C2) were observed at all surface pressures up to collapse. In the opposite limit, for $X_{H16PO_3} \leqslant 0.07$, the mixed monolayer consisted of $H16PO_3$-rich bright domains denoted S1 (solid phase) within a $F8H11PO_3$-rich dark surrounding phase. At high surface pressures, the S1 domains came into close contact and sintered, but did not coalesce, consistent with the designation of this phase as solid. For intermediate mole

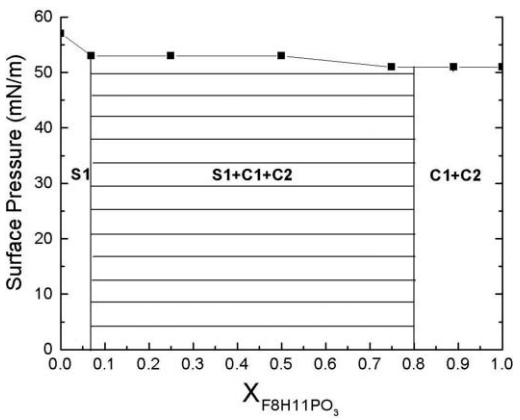

Fig. 1 Monolayer phase diagram of $H16PO_3$/$F8H11PO_3$ mixtures.

fractions, $0.07 \leqslant X_{F8H11PO3} \leqslant 0.8$, the monolayer showed the coexistence of clusters (C1 + C2) and solid phase domains (S1).

Surface-pressure isotherms

Fig. 2 shows isotherms of the surface pressure (Π) as a function of the molecular area (A) obtained for the pure components $H16PO_3$ and $F8H11PO_3$ and their mixtures. For pure $H16PO_3$, Π was negligible during compression until A = 0.22 nm^2. We will show below that this behavior corresponds to the coexistence of the S1 phase and a 2D vapor. At areas below A = 0.22 nm^2 per molecule, Π increased steeply and monotonically until the monolayer collapsed at Π = 57 mN m^{-1}. The isotherm of pure $F8H11PO_3$ began to rise at ~0.28 nm^2 and initially increased more gradually than the hydrocarbon monolayer. There were two noticeable kinks at Π = 9 mN m^{-1} and Π = 15 mN m^{-1}. Presumably, these kinks represent some sort of phase transition; however, we did not observe any characteristic difference in the structure of the monolayer, with BAM or AFM, associated with the isotherm kinks. It is likely that the isotherm features indicate transitions associated with the details of molecular packing that do not result in changes to the mesoscale structure. Isotherms for mixed monolayers displayed intermediate behavior between the two pure components; in particular, the area at which Π began to rise decreased with increasing mole fraction of $H16PO_3$. Further, these isotherms of mixtures also displayed the same distinctive kinks as that of the fluorinated component.

BAM images

Representative BAM images of pure and mixed monolayers are shown in Fig. 3. Pure $H16PO_3$ monolayers (Fig. 3a) displayed small, bright domains at low surface pressure (Π = 0.01 mN m^{-1}). We interpret these images to represent the coexistence of the S1 phase (bright domains) with a 2D vapor phase (dark surroundings). As the monolayer was compressed, the bright domains grew dramatically at the expense of the surrounding dark phase. Fig. 3b shows a

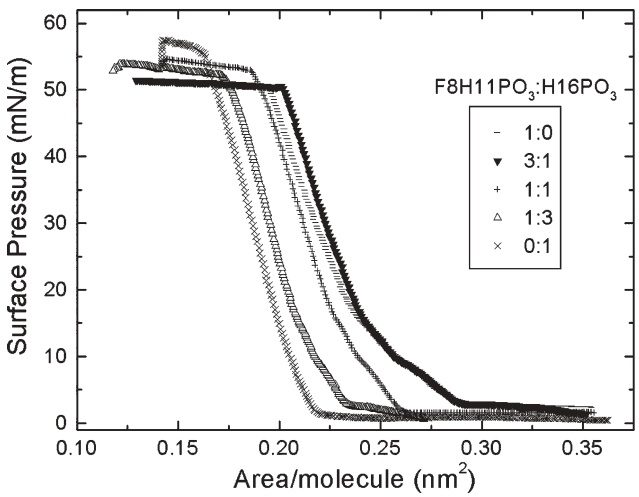

Fig. 2 π-A isotherms of pure $H16PO_3$, $F8H11PO_3$ and their mixtures on a water subphase (pH = 3).

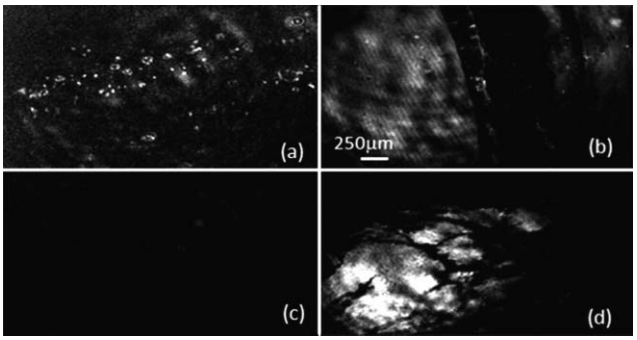

Fig. 3 BAM images of (a) a pure monolayer of $H16PO_3$ at Π = 0.01 mN m^{-1}, (b) a pure monolayer of $H16PO_3$ at Π = 0.14 mN m^{-1}, (c) a pure monolayer of $F8H11PO_3$ and (d) an equimolar-mixed monolayer of $H16PO_3$ and $F8H11PO_3$.

representative BAM image at Π = 0.14 mN m^{-1}. Eventually, the dark phase disappeared completely ($\Pi \sim$ 0.3 mN m^{-1}), and the BAM images appeared uniformly bright until the collapse pressure was reached.

Monolayers of pure $F8H11PO_3$ showed little contrast in their BAM images (Fig. 3c), regardless of surface pressure, due to the fact that the refractive index of fluorocarbons is close to that of water. In fact, for $X_{F8H11PO_3} \geqslant 0.8$, the BAM images were uniform and fairly dark; no bright domains were observed, suggesting that the monolayer was laterally-homogeneous on μm length scales. We will show below, however, that this phase has a distinctive nanostructure discernable with AFM.

For mixed monolayers in the large coexistence region of the phase diagram, the BAM images showed the presence of large, bright domains at all surface pressures up to collapse (Fig. 3d). As the mole fraction of $F8H11PO_3$ was increased in the mixed monolayer, the amount of the bright solid phase decreased significantly, consistent with the phase diagram shown in Fig. 1. A careful analysis of these bright regions suggests that they are composed of small, circular islands that are more easily resolved in the AFM images below.

AFM images

Fig. 4 shows a representative AFM image of a pure $H16PO_3$ monolayer transferred at 4 mN m^{-1}. The surface contained large, flat regions with lines of hole defects. The morphology of the image suggests that domains of the S1 phase failed to coalesce completely as they came together during compression. Analysis of the cross-section showed an average vertical distance of ~1.47 ± 0.1 nm from the monolayer surface to the bottom of the holes, and phase-contrast images (from tapping mode AFM) indicated that the surface at the bottom of the holes had a mechanical response consistent with bare substrate.[20] Thus, the film thickness is smaller than the extended molecular length of $H16PO_3$ (~2 nm) indicating a tilted molecular orientation of $H16PO_3$ in the monolayer at this relatively low surface pressure. This hypothetical molecular tilt is also consistent with the relatively high compressibility of the monolayer and the fact that the molecular area at which the monolayer was deposited (~0.21 nm^2) was significantly larger than the close-packed area of alkyl chains

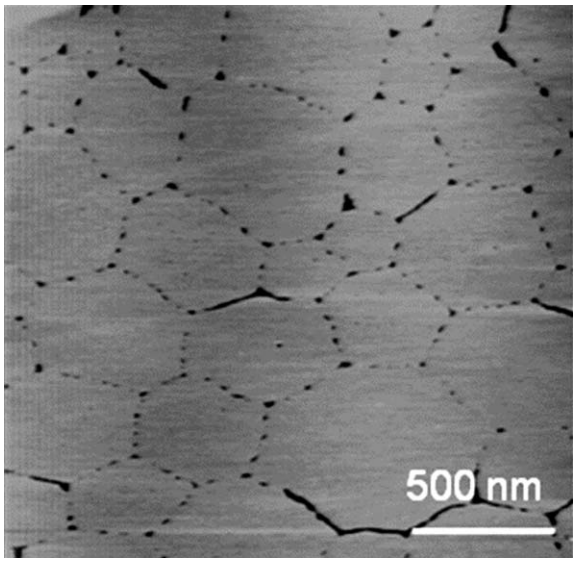

Fig. 4 AFM image of an LB film of pure $H16PO_3$. The monolayer was transferred onto mica at 4 mN m^{-1}.

($\sim$0.18 nm^2). However, the evidence for molecular tilt in the S1 phase is not completely unambiguous. For example, in many tilted monolayer phases, distinctive textures (*e.g.* stars, boojums) can be observed within domains using BAM.[21] No such textures are observed in S1-phase domains. Additionally, one might expect to see a kink in the isotherm associated with the untilted–tilted transition.[22]

Transferred films of the pure semi-fluorinated monolayers, $F8H11PO_3$, at 4 mN m^{-1}, showed the coexistence of two distinctive nanostructures (Fig. 5). In both structures, small features representing molecular clusters were observed, with characteristic dimensions of $\sim$30 nm; however, the shape and arrangement of the clusters was distinctly different in the two cases. Most regions of the film surface were represented by the structure we denote as the C1 phase. C1 clusters are elongated and arranged in regular rows (stripes). The major axis of each cluster is tilted with respect to the row normal. In the minority C2 phase, the clusters are approximately round, and either randomly-ordered or in a local hexagonal arrangement. In both phases, the clusters are extremely monodisperse. We were not able to discern any systematic trend in the appearance of the C2 phase, as a function either of composition or surface pressure. Since, however, this structure was relatively uncommon under all conditions, we focus the remaining discussion on the more prevalent C1 phase.

Representative AFM images corresponding to various regions of an equimolar-mixed monolayer of $H16PO_3$ and $F8H11PO_3$ are shown in Fig. 6. The images in these different regions are consistent with the coexistence of the phases described above. Fig. 6a shows a region consisting of clusters, C1 in this case. Fig. 6b shows a different region of the film that

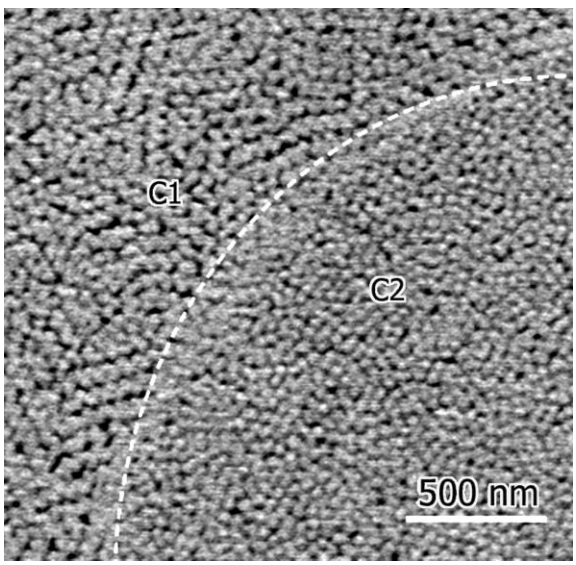

Fig. 5 AFM image of an LB film of $F8H11PO_3$. The monolayer was transferred onto mica at 4 mN m^{-1}. This image shows the coexistence of C1 and C2 clusters.

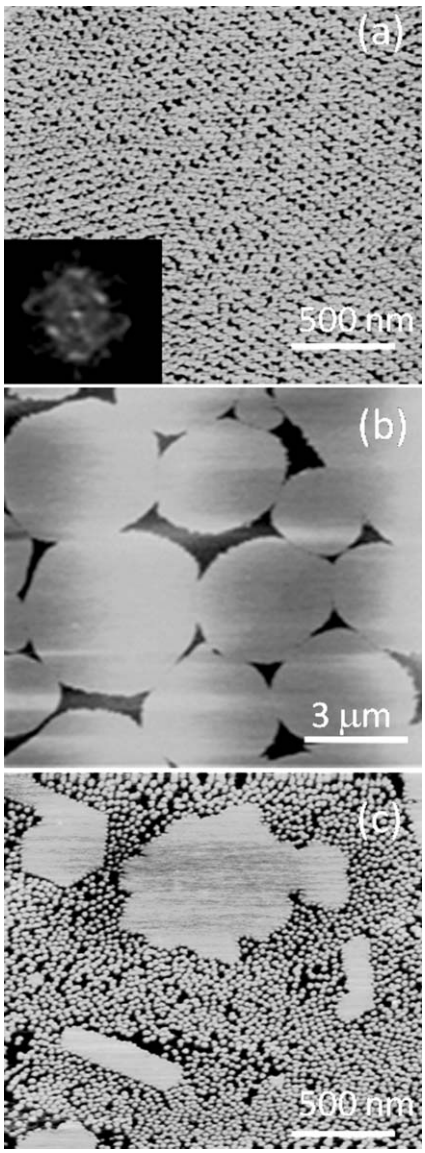

Fig. 6 AFM images of equimolar-mixed monolayer of $H16PO_3$ and $F8H11PO_3$: (a) C1 clusters, (b) S1 phase, and (c) coexistence of S1 phase and C1 clusters.

displays large circular islands of varying size, suggesting a similarity with the S1-phase domains described above. On rare occasions, a region of the surface was encountered (Fig. 6c) that appears to show explicitly the coexistence of a laterally-homogeneous S1 phase and clusters. In this particular image, the S1 regions are relatively small with distinctive faceted shapes.

As described above, one of the major objectives of this research was to understand how the incorporation of a hydrocarbon component might alter the structure of molecular clusters composed of a semi-fluorinated component. The region of the phase diagram for $X_{F8H11PO_3} \geqslant 0.8$ is particularly interesting in this regard, because only the cluster phase is present, but the average composition varies significantly. The most noticeable effect of composition on the cluster phase involved the apparent height of clusters. For example, at $X_{F8H11PO_3} = 0.85$, the height of the clusters was $\sim$0.7 nm. As the mole fraction of $F8H11PO_3$ was decreased to 0.79, however, the cluster height systematically increased to $\sim$1.5 nm. We note that this dimension is the same as the thickness of the S1-phase domains, suggesting that the hydrocarbon component might control the cluster height. Further addition of $H16PO_3$ failed to increase the height of the clusters beyond this value. If we accept the premise of mixed clusters containing both $H16PO_3$ and $F8H11PO_3$, this result suggests that incorporation of $H16PO_3$ into the clusters swelled them in the vertical direction. Presumably, the clusters could accommodate only a certain amount of hydrocarbon, and at mole fractions above $X_{H16PO_3} = 0.2$, the height of the clusters saturated at a constant value. We presume that additional $H16PO_3$ was partitioned into a coexisting phase.

With increasing mole fraction of $H16PO_3$, we also observed an increase in the degree of organization of the clusters. For $X_{F8H11PO_3} > 0.80$, rows or stripes of clusters were clearly visible in AFM images, and a 2D Fourier transform showed distinct spots that are characteristic of these rows (see Fig. 7a). This organization has a liquid-crystalline appearance reminiscent of a smectic phase in 2D. However, for $X_{F8H11PO_3} < 0.80$, the organization of the clusters in the C1 phase improved significantly to the point where crystalline order was readily apparent. Fig. 7b shows a Fourier transform of an AFM image from this regime. Sharp spots in a rectangular arrangement are clearly visible and have been assigned to reciprocal lattice vectors b_1 and b_2. This reciprocal lattice and the real-space images themselves are consistent with the arrangement of clusters shown in Fig. 7c. In this structure, the oblong clusters are arranged in rows that are separated by 50.5 $\pm$ 0.5 nm.

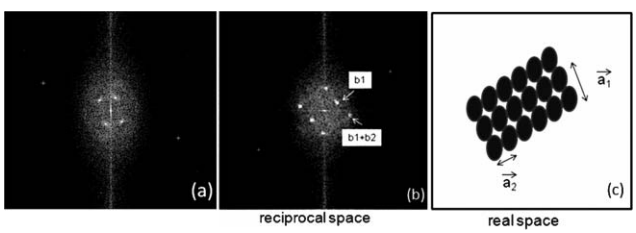

Fig. 7 Two-dimensional Fourier transform spectra of C1 clusters: (a) $X_{F8H11PO_3} > 0.80$ and (b) $X_{F8H11PO_3} < 0.80$. (c) Diagram showing the arrangement of clusters consistent with the rectangular unit cell.

Within a row, the clusters are separated by 41.5 $\pm$ 1.5 nm. The major axis of each cluster is tilted with respect to the row normal; the tilt angle varied from domain to domain within the range 34–64°.

Discussion

Supermolecular organization into discrete assemblies is a general phenomenon associated with bifunctional molecules that consist of dissimilar blocks. Micelles (spherical or cylindrical) of small molecule surfactants[23,24] or diblock copolymers[25] are classic examples. These are equilibrium structures associated with equilibrium conditions, and the characteristic dimension of the assembly is monodisperse and generally associated with a molecular dimension.[15] Thus, as the concentration of the assemblies is increased, there is a tendency for them to pack regularly – long-range order often results, as in lyotropic liquid crystals. The characteristic dimension can often be modified by the addition of a third component that "swells" the surfactant assemblies. Some of these principles have also been demonstrated at interfaces. For example, regular arrays of micelles or reverse micelles form readily at the interface between surfactant solution and a solid surface of the appropriate polarity.[20] The interfacial analog of the "swelling" behavior has not been observed previously.

While the clusters observed in the current work have many characteristics that are similar to the micelles and surface micelles described above, there are also some discrepancies. The lateral dimension of the clusters observed here are significantly larger than any molecular dimension, and they have no discernable curvature, although a subtle molecular splay cannot be ruled out. In these regards, they are reminiscent of equilibrium domains that form in phase-separated monolayers composed of cholesterol and the lipid DPPC.[3] These domains are flat in shape, and the lateral size is much larger than molecular dimensions. The domain shapes and sizes in these lipid mixtures have been interpreted in terms of a competition between line tension at the domain boundaries and dipole–dipole electrostatic repulsion between molecules within and between domains.[26] Similar arguments have been used to explain domains in perfluorinated monolayers.[11] In principle, extremely low values of line tension could lead to nanoscale domains. However, experimentally-observed lipid domains are $\geqslant$1 μm in size, even in the vicinity of the critical point, where the line tension should vanish.

The purely two-dimensional analogue of the aforementioned micellar structures requires a trifunctional molecule in general. For example, a hydrophobic moiety may be used to anchor a molecule at the air–water interface, and two dissimilar hydrophobic blocks (*e.g.*, fluorocarbon and hydrocarbon) may be attached to this headgroup. There are also examples of situations in which a hydrophilic headgroup is not actually required for stable monolayer formation, as in the case of perfluorinated (or partially-perfluorinated) alkanes.[27] Clusters are often observed in this class of monolayer.[15,28] Kato *et al.* observed nanoscale molecular clusters in monolayers of a series of semi-fluorinated long-chain acids.[29] Although the clusters had a characteristic range of sizes, they were not truly monodisperse. Perhaps due to this lack of monodispersity, the

clusters displayed no long-range order. The authors speculated that the clusters were not equilibrium structures, but formed as a result of a spreading instability. However, the characteristic cluster size and shape in these systems have generally been observed to depend systematically on the hydrocarbon and fluorocarbon block lengths,[29] suggesting that the clusters are indeed equilibrium structures. Our observation in the current work – that clusters (of the same size and shape) continue to exist in concert with the excess of another phase – is also consistent with the equilibrium interpretation. We also note that clusters of most amphiphiles fuse upon compression, forming a uniform monolayer. However, the clusters reported here are quite stable and do not fuse even at high surface pressure.

In previous observations of molecular clusters in Langmuir monolayers, long-range organization of the clusters was generally absent, or at least quite rare. We attribute this behavior to the fact that the clusters themselves displayed significant variability of size and shape. In contrast, in the current system, the clusters are extremely uniform, which promotes efficient packing and long-range order, even the complex rectangular C1 phase.

Conclusions

AFM images of a semi-fluorinated phosphonic acid transferred to mica reveal the presence of two-dimensional nanoscale molecular clusters. Two types of clusters are observed: C1 clusters are elongated and arranged in regular rows, and C2 clusters are circular and randomly ordered. We found that the height and organization of the C1 clusters changed systematically upon the addition of a purely hydrocarbon component ($H16PO_3$). In particular, the addition of $H16PO_3$, up to a concentration of $\sim$20%, increased the height of the clusters and converted the long-range order from liquid-crystalline to crystalline. Upon further addition of $H16PO_3$, the height of the clusters saturated, and the additional $H16PO_3$ phase separated.

This work demonstrated that the height and the organization of semi-fluorinated clusters changes upon the addition of a purely hydrocarbon component. We suggest that this behavior can be interpreted as the 2D analog of micelle swelling. Further work is necessary to clarify the influence of the length of the hydrocarbon and the semi-fluorinated segments on the shape, size, and organization of the clusters and to investigate the influence of adding a hydrocarbon component to a series of semi-fluorinated components.

Acknowledgements

This research was supported by NSF awards DMR-0447585 (ST and DKS) and DMR-0447588 (SZ and TRL).

References

1 M. P. Krafft, *Cosmet. Sci. Technol. Ser.*, 1998, **19**, 195.
2 J. G. Riess and M. P. Krafft, *Biomaterials*, 1998, **19**, 1529.
3 R. M. Weis and H. M. McConnell, *J. Phys. Chem.*, 1985, **89**, 4453.
4 M. Jaschke, H. J. Butt, H. E. Gaub and S. Manne, *Langmuir*, 1997, **13**, 1381.
5 I. A. Aksay, M. Trau, S. Manne, I. Honma, N. Yao, L. Zhou, P. Fenter, P. M. Eisenberg and S. M. Gruner, *Science*, 1996, **273**, 892.
6 A. A. Acero, M. Li, A. Anibal, B. Lin, S. A. Rice, M. Goldmann, I. Ben Azouz, A. Goudot and F. Rondelez, *J. Chem. Phys.*, 1993, **99**, 7214.
7 W. A. Ducker and E. J. Wanless, *Langmuir*, 1996, **12**, 5915.
8 M. Nelson, N. Cain, C. E. Taylor, B. M. Ocko, D. L. Gin, S. R. Hammond and D. K. Schwartz, *Langmuir*, 2005, **21**, 9799.
9 N. Cain, J. Van Bogaert, D. L. Gin, S. R. Hammond and D. K. Schwartz, *Langmuir*, 2007, **23**, 482.
10 T. Imae, T. Takeshita and M. Kato, *Langmuir*, 2000, **16**, 612.
11 K.-I. Iimura, T. Shiraku and T. Kato, *Langmuir*, 2002, **18**, 10183.
12 P. Mukerjee and A. Y. S. Yang, *J. Phys. Chem.*, 1976, **80**, 1388.
13 H.-J. Lehmler, M. Jay and P. M. Bummer, *Langmuir*, 2000, **16**, 10161.
14 A. A. Acero, M. Li, A. Anibal, B. Lin, S. A. Rice, M. Goldmann, I. Ben Azouz, A. Goudot and F. Rondelez, *J. Chem. Phys.*, 1993, **99**, 7214.
15 M. Maaloum, P. Muller and M. P. Krafft, *Angew. Chem., Int. Ed.*, 2002, **41**, 4331.
16 O. Shibata and M. P. Krafft, *Langmuir*, 2000, **16**, 10281.
17 M. Broniatowski, N. Romeu and P. Dynarowicz, *J. Phys. Chem. B*, 2006, **110**, 3078.
18 S. Hénon and J. Meunier, *Rev. Sci. Instrum.*, 1991, **62**, 936.
19 D. Hönig and D. Mobius, *J. Phys. Chem.*, 1991, **95**, 4590.
20 S. N. Magonov, V. Elings and M.-H. Whangbo, *Surf. Sci. Lett.*, 1997, **375**, L385.
21 X. Qiu, J. Ruiz-Garcia, K. J. Stine, C. M. Knobler and V. J. Selinger, *Phys. Rev. Lett.*, 1991, **67**, 703.
22 V. M. Kaganer, H. Möhwald and P. Dutta, *Rev. Mod. Phys.*, 1999, **71**, 779.
23 E. J. Wanless and W. A. Ducker, *J. Phys. Chem.*, 1996, **100**, 3207.
24 S. Manne, J. P. Cleveland, H. E. Gaub, G. D. Stucky and P. K. Hansma, *Langmuir*, 1994, **10**, 4409.
25 J. Zhu, A. Eisenberg and R. B. Lennox, *J. Am. Chem. Soc.*, 1991, **113**, 5583.
26 H. M. McConnell, *J. Phys. Chem.*, 1992, **96**, 3167.
27 G. L. Gaines, *Langmuir*, 1991, **7**, 3054.
28 A. Mourran, B. Tartsch, M. Gallyamov, S. Magonov, D. Lambeva, B. I. Ostrovskii, I. P. Dolbnya, W. de jeu and M. Moeller, *Langmuir*, 2005, **21**, 2308.
29 T. Kato, M. Kameyama, M. Ehara and K.-I. Iimura, *Langmuir*, 1998, **14**, 1786.

